Glacial and Structural Geomorphology in the Maladeta Massif, Pyrenees

15

J. Chueca-Cía, A. Julián-Andrés, and M. Ortuño-Candela

Abstract
This work presents the general geomorphological setting of the Maladeta Massif and a more specific analysis on two outstanding aspects of this Alpine area: (1) the main lithostructural features and their relation with active deformation processes (active faults and deep-seated landslides) and (2) the glacial geomorphology of the massif, focusing on the recent recessional pattern (1981–2005) of the glacial masses (glaciers and glacierets). Historical surface and volume losses in the ice bodies are assessed, together with the climatic and topographic factors that have controlled the shrinkage of glaciers at regional and local scales.

Keywords
Glacial geomorphology • Structural geomorphology • Maladeta Massif • Pyrenees

15.1 Introduction

In recent years, several studies have analysed the geomorphology of the Maladeta Massif (Central Spanish Pyrenees), addressing issues related to geomorphological mapping (Chueca and Julián 2008), lithostructural features and their relationship with active gravitational and tectonic deformation (Gutiérrez et al. 2005, 2008; Ortuño 2008; Ortuño et al. 2008; Larrasoaña et al. 2010), or the present-day glacial processes and the evolution of the glaciers since the end of the Little Ice Age (LIA) (Chueca et al. 2003a, 2005, 2007; Chueca and Julián 2004; López-Moreno et al. 2006a, b).

One of the most significant singularities of the Maladeta Massif from the geomorphological perspective is that it hosts the largest glacial complex in the Pyrenees. Since the LIA, the high altitude and the NW–SE trend of the range have favoured the preservation of several N–NE-facing glaciers and glacierets (i.e. small ice masses derived from former glaciers with no signs of displacement). A similar situation is found in other glaciated massifs of the Pyrenees, such as Balaitús, Infiernos, Vignemale, Monte Perdido or Perdiguero. The Aneto glacier in the Maladeta Massif is the largest Pyrenean glacier (79.6 ha as measured in 2005).

This chapter provides a general setting for the Maladeta Massif and analyzes two topics of special geomorphological significance: (1) active deformation processes (active faults and deep-seated landslides) and their relationship with the lithological and structural context and (2) the glacial geomorphology of the range, specially the recent recessional patterns (1981–2005) observed in the glaciers and glacierets. The reduction in surface and volume of the ice bodies is assessed, as well as the controlling factors (climatic and topographic) of the glacial regression, both at regional and local scales.

J. Chueca-Cía (✉)
Departamento de Geografía y Ordenación del Territorio, Facultad de Filosofía y Letras, Universidad de Zaragoza, 50009, Zaragoza, Spain
e-mail: jchueca@unizar.es

A. Julián-Andrés
Departamento de Geografía y Ordenación del Territorio, Escuela Politécnica Superior, Universidad de Zaragoza, 22071, Huesca, Spain
e-mail: ajulian@unizar.es

M. Ortuño-Candela
Departament de Geodinàmica i Geofísica, Facultat de Geologia, Universitat de Barcelona, 08028, Barcelona, Spain
e-mail: maria.ortuno@ub.edu

F. Gutiérrez and M. Gutiérrez (eds.), *Landscapes and Landforms of Spain*, World Geomorphological Landscapes,
DOI: 10.1007/978-94-017-8628-7_15,

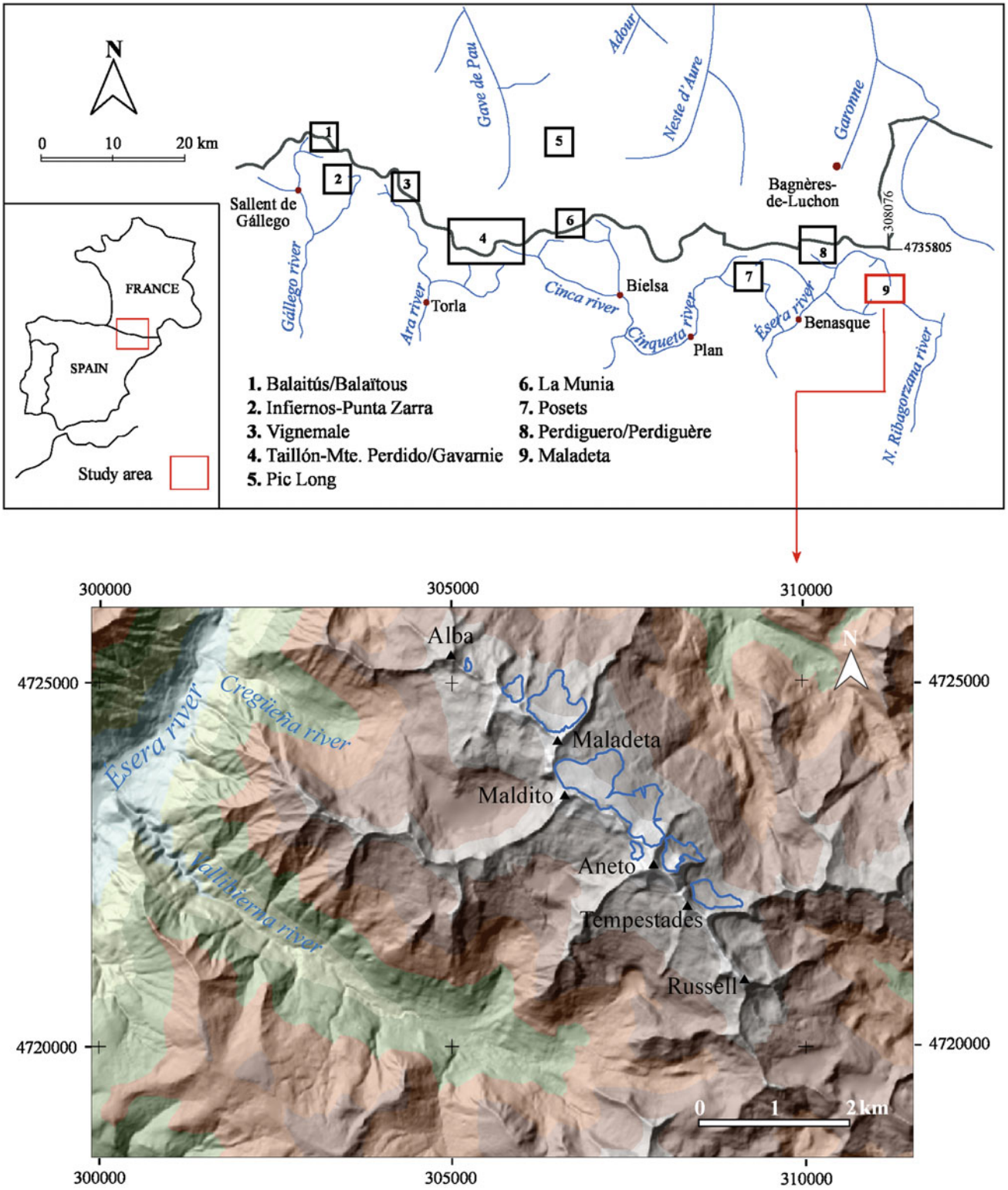

Fig. 15.1 Location of the study area (Maladeta Massif) and the present-day glaciated sectors within the Pyrenees. The lower image depicts the distribution of glaciers and glacierets in the Maladeta Massif in 2005

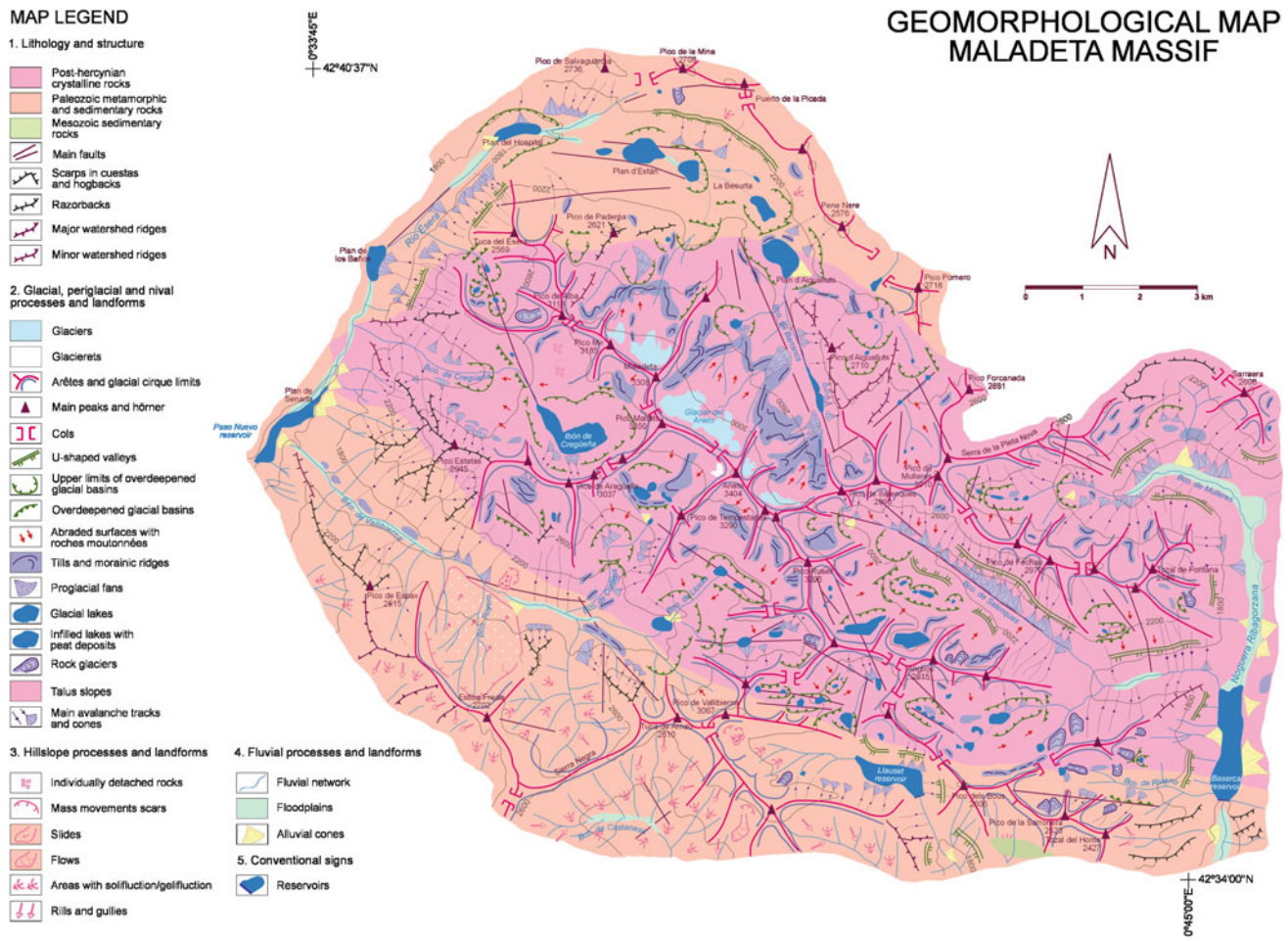

Fig. 15.2 Geomorphological map of the Maladeta Massif

15.2 Study Area

The Maladeta Massif is located in the central Spanish Pyrenees, between the Ésera and Noguera Ribagorzana valleys, and is the highest mountainous area of the Pyrenees (Fig. 15.1). It is formed of crystalline rocks of the Maladeta batholith. This igneous body extends in an E–W direction and consists mainly of homogenous masses of granodiorite and granite. The high altitudes of the massif (e.g. Aneto, 3,404 m a.s.l.; Pico Maldito, 3,350 m; Maladeta, 3,308 m; Tempestades, 3,290 m; Pico Russell, 3,205 m) are largely related to the high resistance to erosion of the massive crystalline bedrock.

The landscape in this sector of the Pyrenees is mainly the result of Pleistocene glacial activity. Limited transformation of the relict glacial landforms has occurred during the Holocene, predominantly by periglacial and mass-wasting processes. The present-day alpine relief is characterized by over-deepened glacial valleys (Alto Ésera, Vallibierna, Salenques, Alta Noguera Ribagorzana) with steep walls. The main landforms in the highest sectors include the following: (1) glacial cirques with abraded surfaces, roches moutonnées, over-deepened basins, glacial lakes and peat bogs associated with infilled lakes; (2) talus slopes; (3) moraine ridges and protalus ramparts corresponding to Neoglacial and LIA periods and (4) small rock glaciers derived from talus deposits with discontinuous permafrost, affected by flow processes (Figs. 15.2, 15.3).

Above the tree line (2,100–2,200 m), slopes are frequently covered by rock debris or till deposits. The mean annual temperature varies from −0.5 °C at 3,000 m to +6.8 °C at 1,500 m. In the coldest month, the average temperature reaches −4.3 °C at 3,000 m and +0.3 °C at 1,500 m. The annual precipitation varies from 2,600 mm at 3,000 m to 1,400 mm at 1,500 m (Chueca and Julián 2004). Discontinuous and sporadic permafrost have been reported

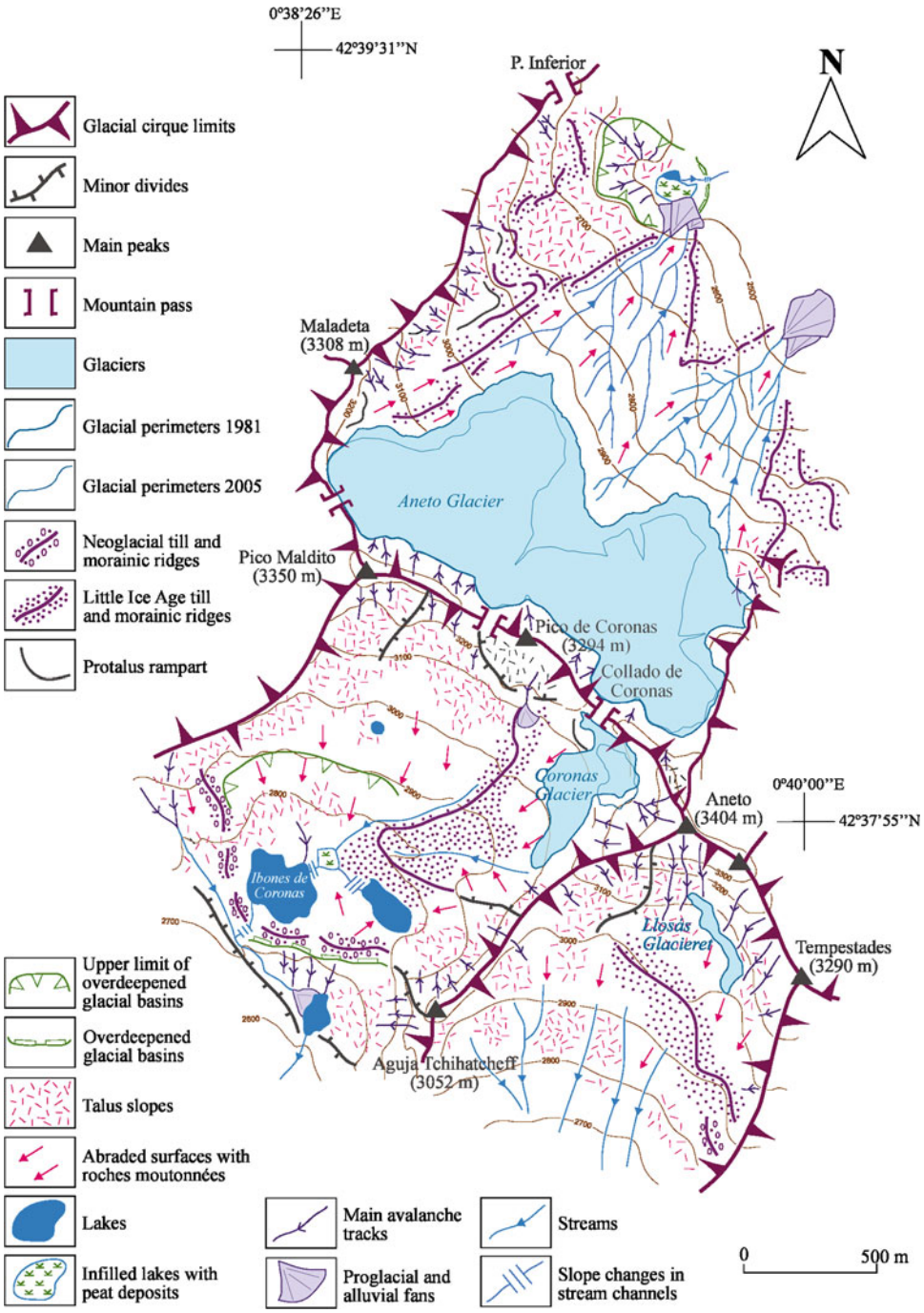

Fig. 15.3 Detailed geomorphological map of the central part of the Maladeta Massif; glacial cirques of Aneto, Coronas and Llosás

in the Maladeta Massif. Detailed studies are restricted to the Aneto glacial cirque area, where thermal characterization of the soil pointed to the probable existence of permafrost in several sectors between 2,950 and 3,050 m, including LIA moraine deposits and protalus ramparts associated with the Aneto glacier and the former Cresta de los Portillones glacier (Chueca and Julián 2010).

15.3 Geomorphology

15.3.1 Lithology and Structure

The lithology and structure of the Maladeta Massif are major factors controlling the development of landforms in the area. The massif is made up of granitoids surrounded by

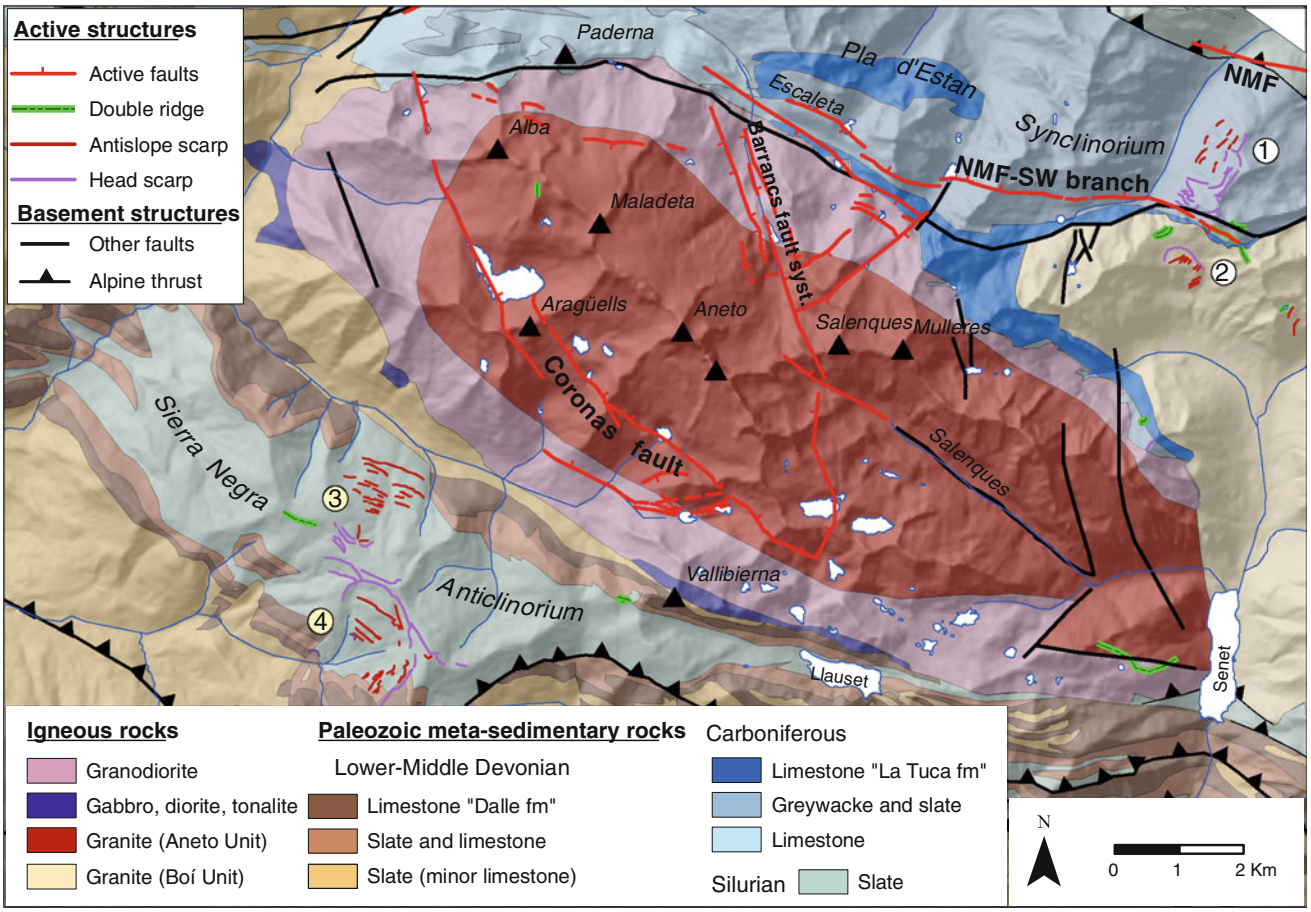

Fig. 15.4 Synthetic sketch of the main lithological units identified in the Maladeta Massif (compiled by Ortuño 2008) using data from Zwart (1979), Arranz (1997) and Ríos et al. (1997). The active faults identified in the area by Ortuño (2008) have been included. NMF: North Maladeta fault. Four conspicuous cases of gravitational slope failure occur in the metamorphic aureole: *1* the Hurno site (Bordonau and Vilaplana 1986); *2* the Mulleres sites (Ortuño 2008); *3* the Vallibierna-Fangonielles site (Lampre 1998; Gutiérrez et al. 2005) and *4* El Ubago site (Gutiérrez et al. 2008)

Paleozoic meta-sedimentary rocks. The area described in this chapter corresponds to the western sector of the Maladeta batholith, emplaced at the end of the Variscan orogeny producing a thermal metamorphic aureole (Charlet 1979; Zwart 1979; García-Sansegundo 1991, 1992; Arranz 1997; Arranz and Lago 2004). The metamorphosed sedimentary rocks surrounding the batholith were intensively folded and faulted during Variscan times. Later, during the Alpine orogeny, these basement rocks were incorporated into the Orry thrust sheet, one of the three structural units of the antiformal stack of the Pyrenean Axial Zone defined by Muñoz (1992).

The Granitic Batholith

Most of the area is dominated by the granodiorites of the Aneto unit, as defined by Charlet (1979) and Arranz (1997). The different lithofacies of this unit display a concentric zonation, with an inner part consisting of granite with two micas and cordierite and an outer zone of granodiorite. Magnetic foliations also display a concentric distribution (Leblanc et al. 1994). Some patches of mafic rocks (gabbro, diorite and tonalite) are identified in peripheral zones (Fig. 15.4). The age of the intrusion has been estimated at 298 ± 2.5 Ma by using the uranium–lead dating method (Gleizes et al. 1997; Evans et al. 1998).

In contrast to other granitic landscapes in the region, the different lithotypes do not display significant variations in rock erodibility, so that lithological changes are scarcely reflected in the erosional landforms (Ortuño 2008). The plutonic rocks are fractured and affected by Alpine thrusts. The most conspicuous Alpine fault is the Coronas fault, associated with a fault breccia up to 10 m wide (Ortuño 2008). The two main fracture sets have NNW and WNW orientations. The geomorphic expression of these discontinuities has been enhanced by glacial and periglacial erosion processes, and some of them have been reactivated as normal faults during the Neotectonic period, which, in the Central Pyrenees, starts in the Middle Miocene (Lacan and

Ortuño 2012). Furthermore, several valleys within the batholith (e.g. Salenques) are controlled by the fracture orientation or major fault zones (Fig. 15.4).

Meta-sedimentary Folded Rocks

The batholith is surrounded by meta-sedimentary rocks of Silurian to Carboniferous age. The Silurian formations are mainly detrital (e.g. slates), while the Devonian and Carboniferous successions also include calcareous units like dolomites and marble (Zwart 1979; Ríos et al. 1997).

Two major E–W structures are distinguished: the Pla d'Estan synclinorium and the Sierra Negra anticlinorium, to the north and south of the massif, respectively (García-Sansegundo 1991, 1992).They are characterized by two Variscan fold generations with E–W oriented subvertical and recumbent axial planes. A gentle foliation and several E–W-trending subvertical fault zones have been recognized and assigned to the Alpine deformational phase.

North of the batholith the carbonate rocks are affected by intense karstification, as the presence of numerous cover and bedrock collapse sinkholes reveals. The Forau de Aigualluts is a bedrock collapse sinkhole more than 100 m long that functions as a ponor. It swallows the flow of the Ésera River, which emerges more than 3 km to the north in France, after traversing the Mediterranean–Atlantic divide through an underground karst system. To the south, the Sierra Negra Anticlinorium displays a conformable topography, in which Silurian black slates underlie the crest of the ridge, and metamorphosed Devonian sandstones, lutites and limestones crop out on its northern and southern flanks (Fig. 15.4).

15.3.2 Active Faults and Deep-Seated Landslides

The slopes of the Maladeta Massif display numerous downhill- and uphill-facing scarps. Most of them are parallel to the contour lines and correspond to erosional landforms controlled by exfoliation joints (Lampre 1998; Ortuño et al. 2008). However, some scarps within the massif correspond to normal active faults attributable to a combination of neotectonics and slow landsliding. Differential uplift of the valley bottom after the glacial retreat has also been suggested by Ortuño (2008) as a probable deformational process at some particular sites (e.g. Barrancs and Vallibierna valleys).

Gravitational deformation processes in the slopes are likely to be triggered by seismic activity. The epicentres of the two most damaging historical earthquakes in the Central Pyrenees are located in this region: the 1373 Ribagorza earthquake (Mw 6.2; Olivera et al. 2006) and the 1923 Vielha earthquake (Mw 5.8; Susagna et al. 1994).

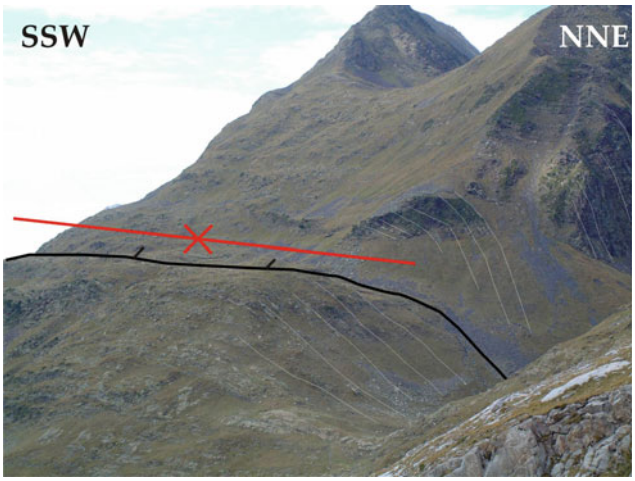

Fig. 15.5 The Escaleta antislope scarp is interpreted as the surface expression of the southwestern branch of the North Maladeta fault. The fault scarp (*black line* with teeth towards the downthrown block) is developed along the axial plane of a tight syncline (the *red line* with a cross in the *middle* shows the fold trace) affecting Carboniferous greywackes and slates

Three active fault systems have been identified in the area: (1) the 7.5-km-long southwestern branch of the North Maladeta fault (NMF); (2) the Barrancs fault system (4.5 km long) and (3) the Coronas fault, 12 km long. The NMF is the most feasible seismic source of the 1923 Vielha earthquake (Ortuño et al. 2008). The location of the 1373 Ribagorza earthquake has an uncertainty of 25 km (Olivera et al. 2006) and could have been produced by the NMF or the Coronas fault, among other faults in the area (Ortuño 2008).

The westernmost segment of the NMF southwestern branch displaces several slopes, coinciding with the axial plane of a tight syncline. This feature is especially conspicuous at the Escaleta site (Figs. 15.4, 15.5). To the south of this site, a group of scarps bounding the Barrancs lake have been interpreted as postglacial normal faults (Moya and Vilaplana 1992; Ortuño 2008). The activity of these faults, which offset polished glacial surfaces (Figs. 15.4, 15.6b), has been related to seismic shaking and could have caused the repeated sudden drainage of the Barrancs lake, as its Holocene sedimentary fill suggests (Larrasoaña et al. 2010).

The most prominent scarp in the area is that of the Coronas fault, developed in the southern flank of the massif (Fig. 15.6c). The fault displaces the slopes carved by glaciers, as attested by the systematic increase in the scarp height towards the centre. To explain the exceptional height of the scarp (more than 120 m), Ortuño (2008) has proposed that the Coronas fault is a composite fault resulting from neotectonic activity and gravitational collapse of the massif towards the north. The collapse is understood as a product by deep-seated gravitational slope deformation involving other structures such us discrete faults observed in the northern

Fig. 15.6 Images of scarps resulting from active deformation on the slopes of the Maladeta Massif and its surroundings. **a** Vallibierna-Fangonielles *sackung* in Sierra Negra range; **b** fault scarps in Barrancs lake offsetting glacially polished surfaces and **c** Coronas fault scarp next to Aragüells peak. The scarp has influenced the distribution of several over-deepening basins related to differential glacial erosion

flank of the massif or the fault system of Barrancs (Fig. 15.4). Glacial over-deepening and karstification at the base of the northern slope, together with topographic amplification of seismic shaking, may have influenced the slope failure.

The presence of *sackung* features in the area, such as double ridges and sets of antislope scarps, frequently associated with landslide head scars on the upper part of the slopes, was first reported in the slopes of the Hurno ridge by Bordonau and Vilaplana (1986). To the south of this ridge, Ortuño (2008) has identified a deep-seated gravitational slope deformation in the Mulleres valley. Two other cases of *sackung* have been reported in the Sierra Negra range: the Vallibierna-Fangonielles (Lampre 1998; Gutiérrez et al. 2005; Fig. 15.6a) and the El Ubago site (Gutiérrez et al. 2008). With the exception of the Mulleres landslide, developed on granitic rocks, the other slope failures occur on foliated metamorphic rocks (Fig. 15.4). The formation of these slow gravitational failures in the Maladeta Massif is likely influenced by the topographic amplification of the seismic waves in the over-steepened slopes. Evidence of episodic activity inferred from trenches excavated across anti-slope scarps in Vallibierna and El Ubago sites led Gutiérrez et al. (2005, 2008) to propose that the episodic activity of these surface ruptures might be related to seismic shaking.

15.3.3 Recent Glacial Evolution

General Setting

Since the end of the LIA, dated in the Pyrenees to ~1820–1830 AD (Chueca and Julián 1996), the Pyrenean glaciers, both in the Spanish and French regions, have experienced significant losses in surface area and volume. At the end of the LIA, the extent of the glaciers in the nine main mountainous massifs (Balaitús, Infiernos, Vignemale, Monte Perdido/Gavarnie, Pic Long, La Munia, Posets, Perdiguero and Maladeta) totalled slightly over 2000 ha, while nowadays, the remaining glacial ice covers 600 ha (Chueca et al. 2004) (Fig. 15.1). In the last two decades of the twentieth century and the beginning of the twenty-first century, glacial shrinkage rates were as high as those estimated for the period 1860–1900 (Chueca et al. 2003a, 2005).

The total extent of the ice masses in the Maladeta Massif reaches 155.0 ha, as measured in 2005 (Chueca et al. 2007), which represents about 25 % of the total area estimated for the final stage of the LIA (616 ha). The largest ice bodies are Aneto (79.6 ha) and eastern Maladeta (36.7 ha) glaciers, while the smallest correspond to Coronas (2.7 ha) and Alba (1.0 ha) glacierets (Figs. 15.2, 15.3). The ice thickness has been estimated by seismic reflection and ground penetrating

radar in the western and eastern Maladeta and Aneto glaciers (Martínez and García 1994; Martínez et al. 1997) and in the Coronas glacieret (Chueca et al. 2003b). According to these geophysical surveys, ice thickness reaches 40–50 m and 7–9 m in the main glaciers and in the Coronas glacieret, respectively.

The glacial bodies included in the study of the recessional pattern (1981–2005) indicated above comprise all the glaciers and glacierets existing in the massif in 1981: Maladeta, Aneto, Barrancs, Tempestades, western Salenques and Coronas glaciers, as well as Alba, eastern Salenques, western and eastern Cregüeña and Llosás glacierets. The extent and volume losses were quantified with a geographical information system (GIS) integrating the results of the following procedures: (1) the analysis of 1981 and 1999 aerial photographs and global positioning system (GPS) measurements conducted in 2005 to quantify ice areal changes and (2) the comparison of digital elevation models of 1981 and 1999 to estimate changes in ice volume (Fig. 15.7). Subsequently, the results were compared with factors that control glacial recession: (1) climatic factors including the evolution of temperature (mean, maximum and minimum) and precipitation during the last decades in the Pyrenean region embracing the Maladeta Massif and (2) local factors related to topography, such as solar radiation inputs, glacier elevation or glacier initial size.

Surface and Volume Losses

The estimated magnitudes of glacier recession are shown in Tables 15.1 and 15.2 and in Fig. 15.8. All glacial bodies display a similar evolution, with clear extent and volumetric losses and increases in the mean altitude of each glacier.

During the period 1981–2005, the glaciers of the Maladeta Massif receded by 35.7 % in surface area, from 240.9 to 155.0 ha. The average surface-loss rate was 3.57 ha/year. Ice volume losses between 1981 and 1999 were estimated at 0.0137 km^3, yielding an average annual rate of 763 × 10^3 m^3/year. Considering an average density for the ice of 0.9 g/cm^3, the ice thickness reduction in the Maladeta Massif was 75.6 m w.e. (water equivalent) (4.2 m w.e./year). Data from glaciers of different extent were compared using the volume loss-to-initial surface ratio (VL/IS) recorded for the period 1981–1999. The VL/SL index value for the whole massif was 5.70 (0.31 VL/IS units/year). Finally, the mean altitude of the studied glaciers increased 43.5 m between 1981 and 2005 (1.81 m/year), from 3026.9 to 3070.4 m a.s.l. This parameter, calculated by averaging the altitudinal value of all pixels classified as glacial surface, was chosen due to its adequacy to evaluate the regression of the small cirque glaciers that characterize the massif. In such glaciers, which may have very irregular geometries, the usual measure of length reduction along one or several axes is less representative than this total value.

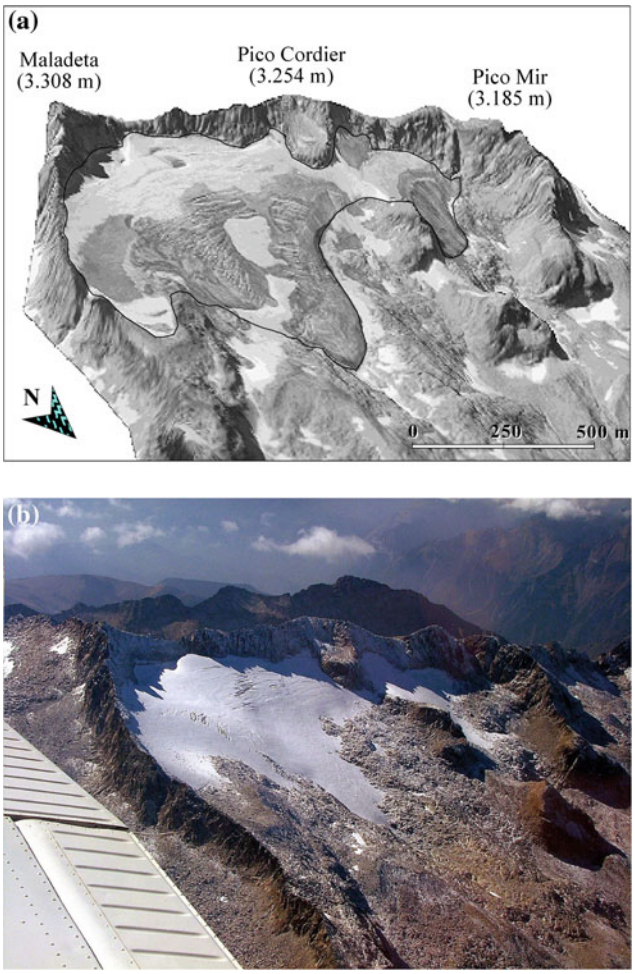

Fig. 15.7 **a** 3-D view of the Maladeta glacier after superimposing the geometrically corrected and georeferenced aerial photograph of the 1981 Pirineos-Sur flight on the 1981 DEM (glacier perimeter is indicated with a black line). **b** Oblique aerial photograph taken in 2005 of the eastern and western Maladeta glaciers. Major ice losses in the small tongue of the eastern Maladeta glacier are obvious

Noticeable differences in the observed shrinkage trends are directly linked to the northern or southern aspect of the studied glaciers and glacierets (Figs. 15.3, 15.8). This effect was quantified by grouping the values of extent and volume losses, and the increase in altitude into two sets: north-facing ice masses (northeast aspect in most cases; Alba, Maladeta, Aneto, Barrancs, Tempestades and western Salenques glacier and eastern Salenques glacieret) and south-facing ice masses (southwest aspect; Coronas glacier and Llosás, western and eastern; Cregüeña glacierets).

Higher volumetric and extent losses and altitudinal changes have been observed in the south-oriented glaciers and glacierets. During the period covered by the study, these glacial bodies decreased in area by 83.9 % (from 16.9 to 2.7 ha), the VL/IS index was 12.28 (0.68 VL/IS units/year) and average altitude in the case of Coronas glacier increased 75 m (3.12 m/year), from 3,081 to 3,156 m a.s.l.

Table 15.1 Volumetric and extent losses in the glaciers of the Maladeta Massif

	Vol. losses 1981–1999 (m^3)	Mean thickness losses 1981–1999 (m w.e.)	Extent 1981 (m^2)	Extent 2005 (m^2)	% Surface loss 1981–2005	VL/IS index
Alba	0.120×10^6	4.1	2.679×10^4	1.004×10^4	62.52	4.51
Maladeta	2.621×10^6	4.9	48.904×10^4	43.028×10^4 $(6.309 + 36.718) \times 10^4$	12.02	5.35
Aneto	4.736×10^6	4.1	106.770×10^4	79.699×10^4	25.36	4.43
Barrancs	1.190×10^6	4.8	22.497×10^4	13.956×10^4	37.97	5.29
Tempestades	2.051×10^6	8.4	28.792×10^4	14.564×10^4	49.42	7.12
Salenques west	0.896×10^6	6.3	12.844×10^4	–	100.00	6.98
Salenques east	0.048×10^6	2.9	1.523×10^4	–	100.00	3.17
Cregüeña west	0.202×10^6	7.9	1.994×10^4	–	100.00	10.15
Cregüeña east	0.229×10^6	10.4	2.344×10^4	–	100.00	9.77
Coronas	1.445×10^6	12.6	10.570×10^4	2.748×10^4	74.00	13.67
Llosás	0.208×10^6	9.2	2.072×10^4	–	100.00	10.08
Total	13.751×10^6	75.6	240.993×10^4	155.002×10^4	–	–

The percentage of surface loss in the Maladeta glacier was calculated after adding the 2005 extent of its two present-day fragments: western and eastern Maladeta glaciers

Table 15.2 Maximum, minimum and mean altitude (m a.s.l) of Maladeta Massif glaciers

	Max. alt. 1981	Min. alt. 1981	Mean alt. 1981	Max. alt. 2005	Min. alt. 2005	Mean alt. 2005	Increase in mean alt. 1981–2005
Alba	3,039	2,923	2,970	3,038	2,950	2,992	22
Maladeta	3,206	2,801	3,051	3,196	2,884	3,061.5	10.5
Aneto	3,325	2,855	3,101	3,316	2,911	3,126	25
Barrancs	3,332	2,899	3,080	3,323	2,938	3,121	41
Tempestades	3,085	2,792	2,928	3,070	2,890	2,966	38
Salenques west	3,122	2,854	2,988	–	–	–	–
Salenques east	2,990	2,877	2,918	–	–	–	–
Cregüeña west	3,021	2,928	2,964	–	–	–	–
Cregüeña east	3,215	3,110	3,146	–	–	–	–
Coronas	3,213	2,984	3,081	3,206	3,100	3,156	75
Llosás	3,108	3,001	3,069	–	–	–	–

The 2005 value for the Maladeta glacier was obtained averaging the altitudes of its two present-day fragments: western and eastern Maladeta glaciers

The other south-oriented ice masses underwent total degradation, and thus, their altitudinal migration is not calculable. The north-facing glaciers diminished their surfaces by 32.1 % (from 224.0 to 152.2 ha), had a VL/IS index of 5.20 (0.28 VL/IS units/year) and their average altitude increased by 48.2 m (2 m/year), from 3,005 m to 3,053 m a.s.l. Only the western Salenques glacier and eastern Salenques glacieret showed complete degradation (Fig. 15.9).

Causes of Recent Glacial Degradation

Analysis of precipitation and temperature trends in the study area reveals a deterioration of conditions favourable for the development of glaciers during the 1980s, 1990s and beginning of the 2000s (Chueca et al. 2007). Snow precipitation during the accumulation period decreased significantly, reducing the snowfall contribution to mass balance in February and March. In addition, an increase in temperature during the ablation season, particularly maximum temperatures, which exert a major influence on ice melting processes (Singh and Singh 2001), also contributed to reinforce negative glacial mass balance.

The rates of glacial degradation over the 1981–2005 period were as high as those estimated for the period 1860–1900 (Chueca et al. 2003a, 2005). Data from the beginning of the twenty-first century indicate a continuation of the negative conditions for glacier conservation. Climatic

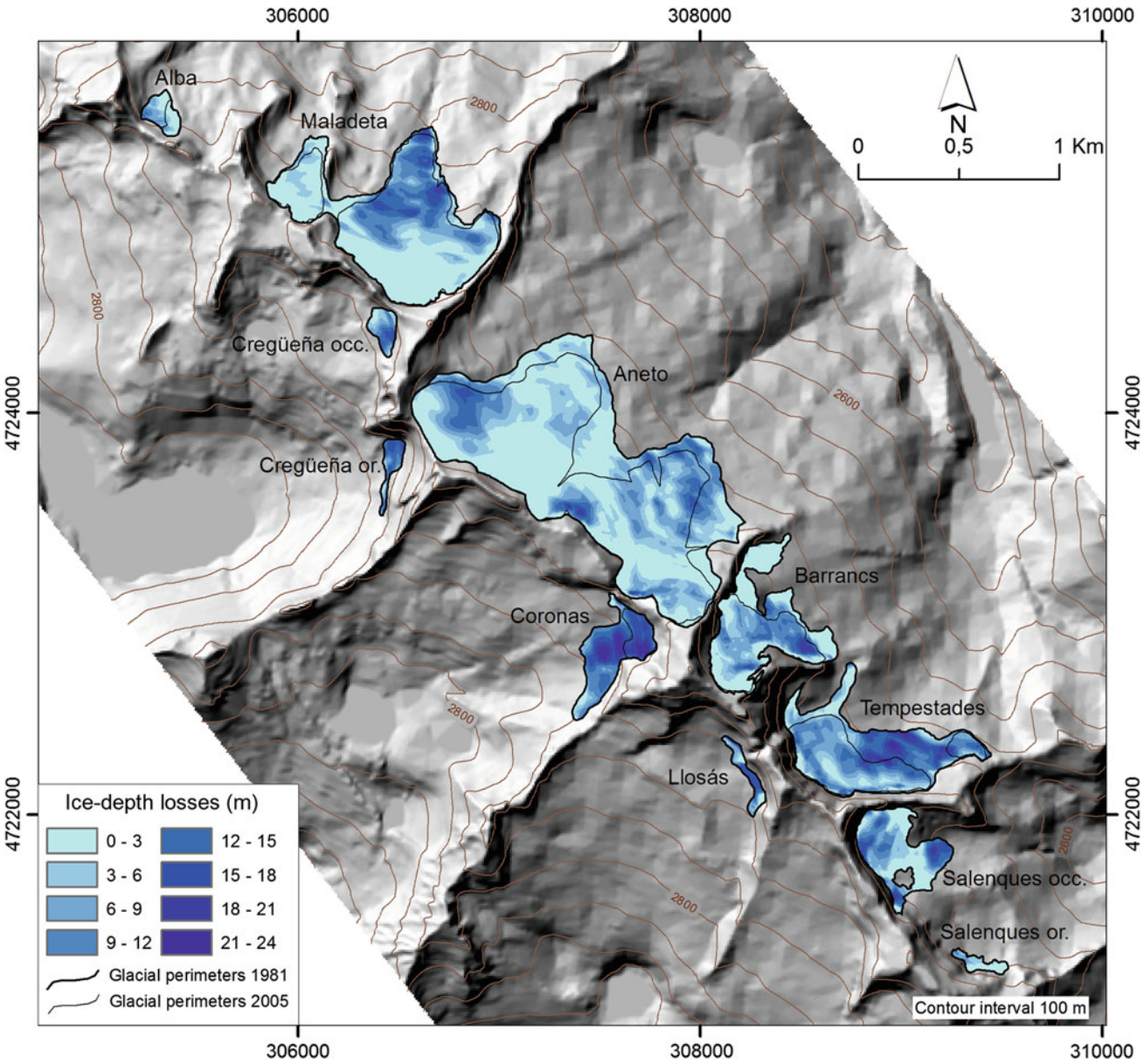

Fig. 15.8 Extent losses (glacier perimeters in 1981 and 2005 are indicated) and ice-depth losses (for the 1981–1999 period) observed in the glaciers and glacierets of the Maladeta Massif

Table 15.3 Correlation coefficients (R) between selected variables and significance level

Variables		R	Significance level
VL/IS index	Mean summer solar radiation	0.77	0.005
VL/IS index	Mean annual solar radiation	0.82	0.002
VL/IS index	Mean initial altitude (1981)	0.35	0.297
VL/IS index	Initial size (1981)	−0.38	0.248
% Surface loss	Initial size (1981)	−0.75	0.008
% Surface loss	Mean summer solar radiation	0.18	0.606
% Surface loss	Mean annual solar radiation	0.34	0.303
Increase mean alt.	Mean summer solar radiation	0.74	0.048
Increase mean alt.	Mean annual solar radiation	0.80	0.028

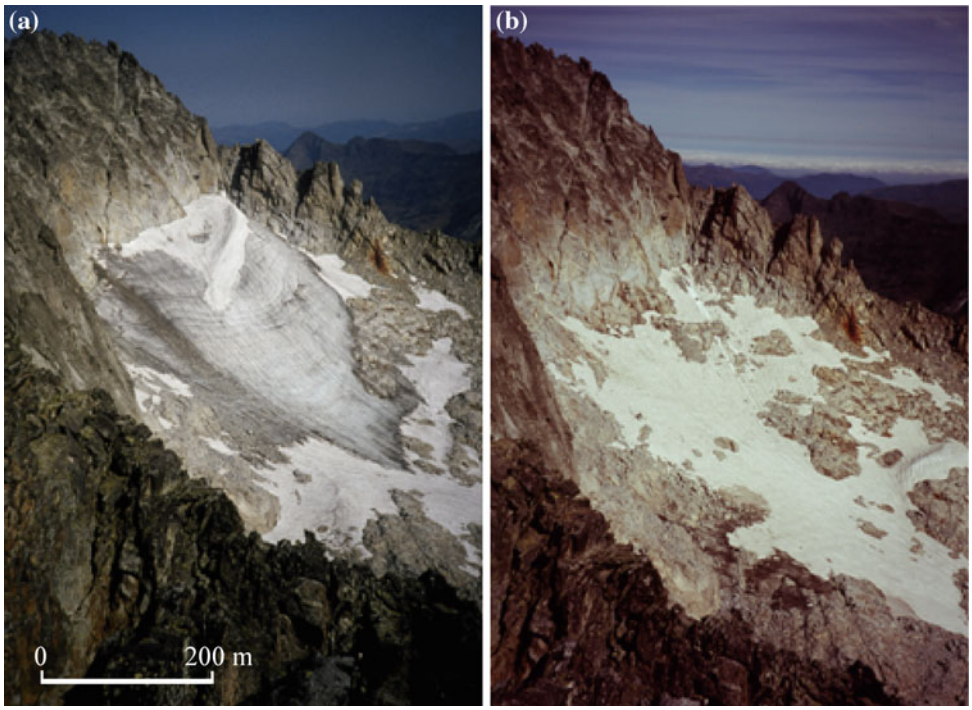

Fig. 15.9 Comparison of the western Salenques glacier in 1990 (**a**) and 2005 (**b**) (*Photographs* by J. Camins)

projections for the twenty-first century (Houghton et al. 2001) in the Mediterranean mountain regions predict an increase in thermal values and a diminution of precipitation that would induce a further deterioration of glacial mass balance.

According to the results of the bivariate correlation analysis (Table 15.3), the three main topographical factors that influence glacial degradation include the following: (1) glacier orientation, which controls to a great extent solar radiation input; (2) glacier altitude and (3) glacier initial size (i.e. extent in 1981). The presence of a debris cover, related either to endoglacial material brought to the ice surface or to rockfalls, can considerably reduce ablation processes on a glacial surface due to its insulating effect. This factor is so far negligible in the Maladeta ice bodies. However, debris cover will probably gain importance in the future, since some of the glaciers and glacierets are beginning to show accumulations of debris on their distal sectors (e.g. western and eastern Maladeta, Barrancs and western Tempestades glaciers, and Coronas glacieret).

Potential incoming solar radiation, in terms of both the summer and annual values, seems to be the main factor that controls the volume loss per surface unit recorded in the glaciers of the Maladeta Massif, as well as the increase in mean altitude derived from their deterioration. As the trends shown in Fig. 15.10a–d illustrate, the higher the solar radiation inputs, the higher the loss of volume per unit area and the higher the increase in the mean altitude of each glacier. This finding is consistent with the previous observations in the study area. López-Moreno et al. (2006b) studied how the influence of topography on the extent of the Maladeta cirque glaciers has changed since the LIA. They found that during the final stages of glacial degradation process, the relative influence of climatic factors linked to altitude (e.g. temperature lapse rate, amount of precipitation and snowfall versus rainfall ratio) decreases with respect to the influence of the exposure to solar radiation and other topography-related variables (e.g. terrain curvature).

Bivariate correlation analyses also confirm the important role of the initial size of glaciers in the subsequent shrinkage process. In the Maladeta Massif, higher rates of surface loss are associated with smaller glaciers and vice versa (Fig. 15.10e). This finding highlights the marked sensitivity of smaller glaciers, which usually have a reduced altitude range, to changes in the main climatic factors. The latter always exhibit a strong altitudinal gradient and thus play a significant role in the accumulation and ablation processes. Chueca et al. (2005) pointed out that there seems to be a minimum response time of a few years between temperature and precipitation changes and the shrinkage of glaciers in the Maladeta Massif. As the response time of a glacier to climatic fluctuations depends mainly on its size and latitudinal location, climatic changes, even if subtle, have a faster effect on the mass balance of small glaciers located in

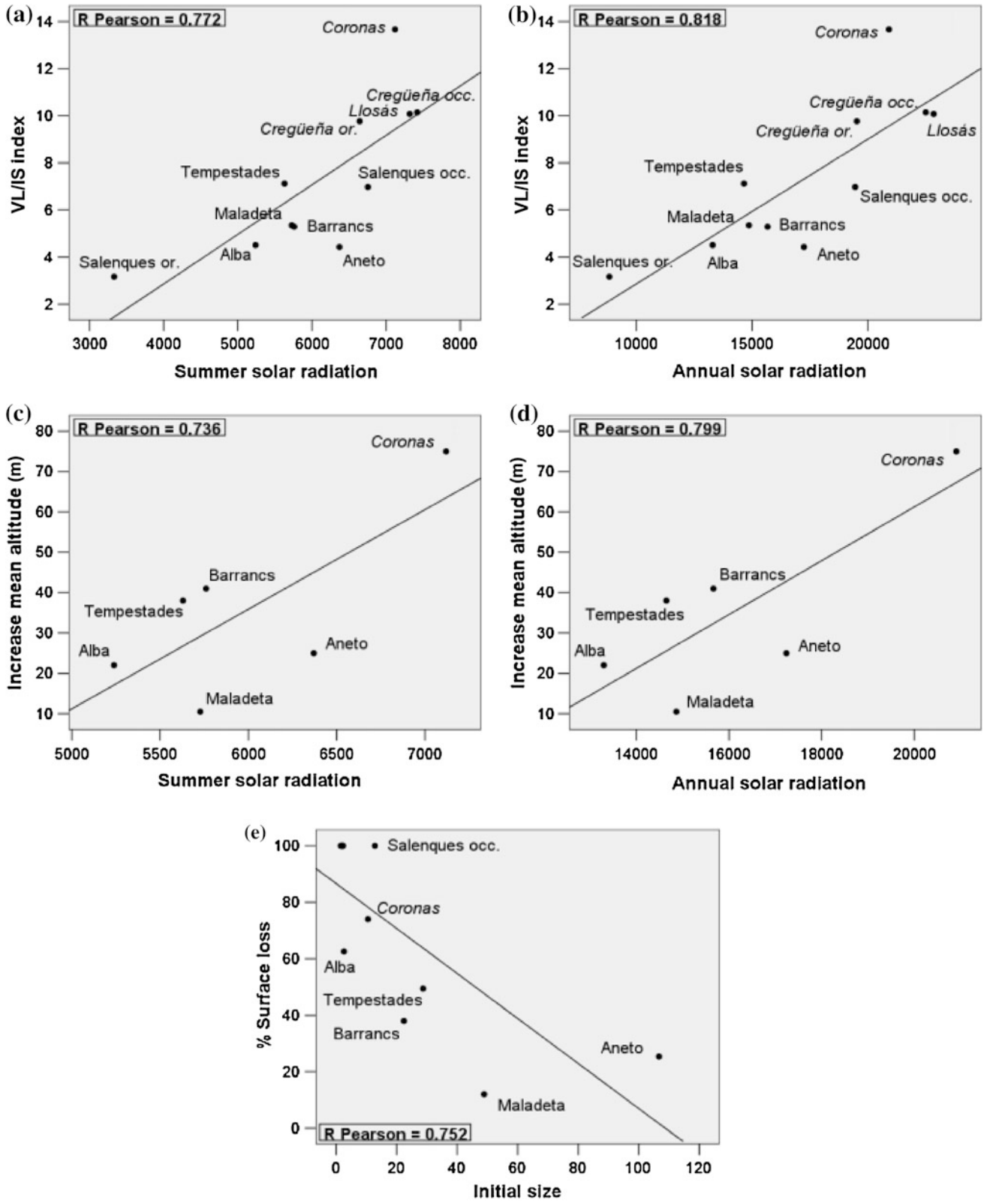

Fig. 15.10 Scatterplots of the relationships between **a** summer solar radiation (10 kJ m^{-2} d^{-1} μm^{-1}) and VL/IS index, **b** annual solar radiation (10 kJ m^{-2} d^{-1} μm^{-1}) and VL/IS index, **c** summer solar radiation (10 kJ m^{-2} d^{-1} μm^{-1}) and increase in mean altitude (1981–2005) (m), **d** annual solar radiation (10 kJ m^{-2} d^{-1} μm^{-1}) and increase in mean altitude (1981–2005) (m), and **e** glacier area in 1981 (ha) and percentage of surface loss (1981–2005). Cases of 100 % surface loss located in the *upper left* include eastern Salenques, western and eastern Cregüeña, and Llosás glaciers. South-oriented glaciers and glacierets are indicated in italics

warmer settings like the Pyrenees, than on larger glaciers at higher latitudes. This fact makes the Pyrenean glacial remnants useful proxies to monitor future climatic changes in mid-latitude mountains.

15.4 Conclusions

The Maladeta granitic massif, including the highest peaks of the Pyrenees, displays remarkable glacial and periglacial landforms, as well as a particularly high density of uphill- and downhill-facing fault scarps attributable to seismogenic active tectonic faults, gravitational deformation (sackung), differential erosion or a combination of these processes.

An outstanding feature of the Maladeta Massif is that it contains some of the southernmost glaciers in Europe. The high rates of volumetric and extent losses that have been observed in the glacial masses (glaciers and glacierets) from 1981 to 2005 are consistent with those detected on a global scale (Haeberli et al. 2005) and in other alpine sectors of the world with variable altitudinal and latitudinal distribution. These changes have been interpreted primarily as a result of the climatic trend observed in this Pyrenean region since the 1980s: a reduction in snowfall and an increase in maximum temperatures. Nevertheless, there are significant differences in the magnitude of these changes, which appear to be related to three factors: the exposure, which controls the input of solar radiation, the altitude, and the initial size of each glacier or glacieret.

If the climatic scenarios predicted for the twenty-first century in this region are correct, the conservation of the fragile Pyrenean glaciers is in danger, and it is reasonable to expect their accelerated degradation and complete disappearance within the next few decades.

References

Arranz E (1997) Petrología del macizo granítico de La Maladeta (Huesca-Lérida): estructura, mineralogía, geoquímica y petrogénesis. Unpublished PhD thesis. Universidad de Zaragoza, Zaragoza

Arranz E, Lago M (2004) El plutonismo sin- y tardi-varisco en los Pirineos. In: Vera JA (ed) Geología de España. SGE-IGME, Madrid, pp 263–266

Bordonau J, Vilaplana JM (1986) Géomorphologie et tectonique récente dans le Val d'Aran (Zone Axiale des Pyrénées Centrales, Espagne). Rev Géologie Dyn Géog Phys 27:303–310

Charlet JM (1979) Le massif granitique de la Maladeta (Pyrénées centrales espagnoles), synthèse des données géologiques. Ann Soc Géol Belgique 102:313–323

Chueca J, Julián A (1996) Datación de depósitos morrénicos de la Pequeña Edad del Hielo: macizo de la Maladeta. In: Pérez Alberti A, Martini P, Chesworth W, Martínez Cortizas A (eds) Dinámica y evolución de Medios Cuaternarios. Xunta de Galicia, Santiago de Compostela, pp 171–182

Chueca J, Julián A (2004) Relationship between solar radiation and the development and morphology of small cirque glaciers (Maladeta mountain massif, Central Pyrenees, Spain). Geogr Ann 86(1):81–89

Chueca J, Julián A (2008) Geomorphological map of the Alta Ribagorza (Central Pyrenees, Spain). J Maps 1:235–247

Chueca J, Julián A (2010) Caracterización térmica del suelo en el circo del Aneto (Pirineo central aragonés: cartografía de variaciones estacionales). In: Blanco JJ, de Pablo MA, Ramos M (eds) Ambientes periglaciares, permafrost y variabilidad climática. Universidad de Alcalá, Alcalá de Henares, pp 55–60

Chueca J, Julián A, López-Moreno JI (2003a) Variations of Glaciar Coronas, Pyrenees, Spain, during the 20th century. J Glaciol 49(166):449–455

Chueca J, López-Moreno JI, Julián A (2003b) Determinación de espesores en el glaciar-helero de Coronas (macizo de la Maladeta; Pirineo central español) mediante el empleo de geo-radar. Boletín Glaciológico Aragonés 4:111–124

Chueca J, Julián A, René P (2004) Estado de los glaciares en la cordillera pirenaica (vertientes española y francesa) a finales del siglo XX. In: Benito G, Díez Herrero A (eds) Contribuciones recientes sobre geomorfología (Actas VIII Reunión Nacional de Geomorfología). SEG-CSIC, Madrid, pp 91–102

Chueca J, Julián A, Saz MA, Creus J, López-Moreno JI (2005) Responses to climatic changes since the Little Ice Age on Maladeta Glacier (Central Pyrenees). Geomorphology 68:167–182

Chueca J, Julián A, López-Moreno JI (2007) Recent evolution (1981–2005) of the Maladeta glaciers, Pyrenees, Spain: extent and volume losses and their relation with climatic and topographic factors. J Glaciol 53(183):547–557

Evans NG, Gleizes G, Leblanc D, Bouchez JL (1998) Syntectonic emplacement of the Maladeta granite (Pyrenees) deduced from relationships between Hercynian deformations and contact metamorphism. J Geol Soc 155:209–216

García-Sansegundo J (1991) Estratigrafía y estructura de la Zona Axial pirenaica en la transversal del Valle de Arán y de la Alta Ribagorza (Parte I). Boletín Geológico y Minero 102:781–829

García-Sansegundo J (1992) Estratigrafía y estructura de la Zona Axial pirenaica en la transversal del Valle de Arán y de la Alta Ribagorza (Parte II). Boletín Geológico y Minero 103:42–93

Gleizes G, Leblanc D, Bouchez JL (1997) Variscan granites of the Pyrenees revisited: their role syntectonic markes of the orogen. Terra Nova 9(1):38–41

Gutiérrez F, Acosta E, Rios S, Guerrero J, Lucha P (2005) Geomorphology and geochronology of sackung features (uphill-facing scarps) in the Central Spanish Pyrenees. Geomorphology 69:298–314

Gutiérrez F, Ortuño M, Lucha P, Guerrero J, Acosta E, Coratza P, Piacentini D, Soldati M, Beguería S (2008) Late Quaternary episodic displacement on a sackung scarp in the central Spanish Pyrenees. Secondary paleoseismic evidence? Geodin Acta 21:187–202

Haeberli W, Zemp M, Frauenfelder R, Hoelzle M, Kääb A (eds) (2005) Fluctuations of glaciers 1995–2000, vol III. World Glacier Monitoring Service, Zurich

Houghton JT, Ding DJ, Griggs M, Noguer M, Van der Linden PJ, Dai X, Maskell K, Johnson CA (eds) (2001) Climate change 2001: the scientific basis. Contribution of working Group I to the Third Assessment Report of the intergovernmental panel on climate change. Cambridge University Press, New York

Lacan P, Ortuño M (2012) Active Tectonics of the Pyrenees: a review. J Iberian Geol 38(1):9–30

Lampre F (1998) Estudio geomorfológico de Ballibierna (Macizo de la Maladeta, Pirineo Aragonés): modelado glacial y periglacial. Consejo de Protección de la Naturaleza, Zaragoza

Larrasoaña JC, Ortuño M, Birks H, Valero-Garcés B, Parés JM, Copons R, Camarero L, Bordonau J (2010) Paleoenvironmental and palaeoseismic implications of a 3,700-year sedimentary record from proglacial Lake Barrancs (Maladeta Massif, Central Pyrenees, Spain). Palaeogeogr Palaeoclimatol Palaeoecol (Palaeo3) 294:83–93

Leblanc D, Gleizes G, Bouchez JL (1994) The Maladeta granite polydiapir, Spanish Pyrenees: a detailed magnetostructural study. J Struct Geol 16:223–235

López-Moreno JI, Nogués D, Chueca J, Julián A (2006a) Glacier development and topographic context. Earth Surf Proc Land 31(12):1585–1594

López-Moreno JI, Nogués D, Chueca J, Julián A (2006b) Change of topographic control on the extent of cirque glaciers since the Little Ice Age. Geophys Res Lett 33:L24505

Martínez R, García F (1994) Trabajos de glaciología en el glaciar de la Maladeta. Campaña 1991–1992. In: MOPTMA (ed) La nieve en las cordilleras españolas. MOPTMA, Madrid, pp 209–236

Martínez R, García F, Macheret Y, Navarro J, Bisbal L (1997) El sustrato subglaciar y la estructura interna de los glaciares del Aneto y la Maladeta cartografiados por geo-radar de ultra-alta frecuencia (UHF). In: MMA (ed) La nieve en las cordilleras españolas. Ministerio de Medio Ambiente, Madrid, pp 227–249

Moya J, Vilaplana JM (1992) Tectónica reciente en el Macizo de la Maladeta, sector del Alto Ésera (Pirineo Central). In: Cearreta A, Ugarte FM (eds) The late Quaternary in the Western Pyrenean region. Universidad del País Vasco, Vitoria, pp 385–403

Muñoz JA (1992) Evolution of a continental collision belt: ECORS-Pyrenees crustal balanced cross-section. In: McClay KR (ed) Thrust tectonics. Chapman and Hall, London, pp 235–246

Olivera C, Redondo E, Lambert J, Riera Melis A, Roca A (2006) Els terratrèmols dels segles XIV i XV a Catalunya. Institut Cartogràfic de Catalunya, Monografies n°30

Ortuño M (2008) Deformación activa en el Pirineo Central: la falla Norte de la Maladeta y otras fallas activas. Unpublished PhD thesis, Universitat de Barcelona, Barcelona

Ortuño M, Queralt P, Martí A, Ledo J, Masana E, Perea H, Santanach P (2008) The North Maladeta Fault (Spanish Central Pyrenees) as the Vielha 1923 earthquake seismic source: recent activity revealed by geomorphological and geophysical research. Tectonophysics 453:246–262

Ríos LM, Galera JM, Barettino D, Charlet JM (1997) Mapa Geológico de España E. 1:50.000, Hoja n° 180 (Benasque). Instituto Geológico y Minero de España, Madrid

Singh P, Singh VP (2001) Snow and glacier hydrology. Kluwer, Dordrecht

Susagna T, Roca A, Goula X, Batlló J (1994) Analysis of macroseismic and instrumental data for the study of the 19 November 1923 earthquake in the Aran Valley (Central Pyrenees). Nat Hazards 10:7–17

Zwart HJ (1979) The geology of the central Pyrenees. Leid Geol Meded 50:1–74